Audio Engineering Society

Convention Paper

Presented at the 138th Convention
2015 May 7–10 Warsaw, Poland

Estimation of the radiation pattern of a violin during the performance using plenacoustic methods

Antonio Canclini[1], Luca Mucci[1], Fabio Antonacci [1], Augusto Sarti [1], and Stefano Tubaro [1]

[1] *Politecnico di Milano, Dipartimento di Elettronica, Informazione e Bioingegneria, Milano, Italy*

Correspondence should be addressed to Antonio Canclini (antonio.canclini@polimi.it)

ABSTRACT

We propose a method for estimating the 3D radiation pattern of violins, during the performance of a musician. A rectangular array of 32 microphones is adopted for measuring the energy radiated by the violin in the observed directions. In order to gather measurements from all the 3D angular directions, the musician is free to move and rotate in front of the array. The position and orientation of the violin is estimated through a tracking system. As the adopted hardware is very compact and non-invasive, the musician plays in a natural fashion, thus replicating the radiation conditions of a real scenario. The experimental results prove the accuracy and the effectiveness of the method.

1. INTRODUCTION

The acoustics of the violin can be analyzed by means of several properties. Of particular interest is the angular dependency of the sound energy radiated from the instrument in the far field, also called *directivity* or *radiation pattern*. The knowledge of the radiation pattern is important to determine the preferred directions of emission of the instrument, which enable to infer how the sound will interact with the environment and therefore how the audience will perceive it. The radiation pattern of the violin is a complex function that depends on several factors (e.g., materials and shapes), and it is difficult to predict. For instance, even small variations in positioning the sound post highly impact on vibration and thus on the sound radiation [1]. Consequently, the pattern significantly differs from one violin to another, even if they are almost identical.

Many methods in the literature addressed the problem of determining the directivity of violins. Weinreich contributed to the study of acoustic models

useful to predict some general radiation characteristics [2]. Moreover, his studies introduced some theoretical aspects about the "directional tone color" phenomenon [3], which cause each note (even within a vibrato) to be perceived as coming from a different direction. Bissinger [4] investigated on the relationship between the main plate modes and the violin radiativity profile.

Alongside the aforementioned theoretical investigations, several measurement techniques were proposed in the last thirty years. Most of them are based on artificial excitation mechanisms: in [2, 3, 5] loudspeakers are adopted for exciting the violin; a force hammer is used in [6]; while the method in [7] relies on a mechanical bowing machine. Despite being characterized by a controlled and repeatable excitation of the instrument, these methods do not consider the effect of human body on sound radiation.

In order to account for the modifications introduced by the human body, other systems measure the directivity pattern of an instrument played by a violinist. In [8] a large semicircular microphone array is used to measure the sound radiated by a violin, while the player sits on a rotating stool. In [9] the musician stands at the center of an anechoic room, holding the violin in a prescribed position, and the acoustic energy is measured at 22 points surrounding it. A similar approach is followed in [10], where a scanning probe microphone is used to measure the soundfield over planar regions. In [11] the violin is kept still on a rigid structure, so that its orientation with respect to the microphone array can be accurately determined. Unfortunately, this solution prevents the musician to play in a natural fashion.

All the mentioned techniques rely on measurements conducted in anechoic rooms, which ensure to capture the sole direct sound radiation. While this scenario is ideal in case of artificial excitation mechanisms, it presents some issues when the instrument is played by a musician. Indeed, it is well known that people could experience psychological issues (e.g., apprehension, anxiety, etc.) when staying in anechoic rooms for moderately long periods. Moreover, the total absence of echoes exposes the player only to the dry violin sound, which typically provokes an annoying sensation that may impact on the naturalness of the performance.

In this paper we propose a novel technique for measuring the 3D radiation pattern of a violin, at all the frequencies of interest. A compact rectangular microphone array (plenacoustic camera) is used to sense the directional components of the wave field. This is accomplished by the plenacoustic analysis of the wavefield proposed in [12], useful to estimate the directional acoustic energy at multiple points in space. This analysis is based on beamforming, and enables the measurement of the radiation pattern even in mildly reverberant rooms. A simple tracking system, composed of a depth map camera and a wireless gyroscope, is used to track the position and the orientation of the musician with respect to the microphones. Each pose assumed by the violinist contributes to the portion of radiation pattern corresponding to the part of the instrument "exposed" to the plenacoustic camera. During the musical performance, the violinist freely moves and rotates in front of the camera, in order to cover the complete 3D angular domain. Similarly to the method in [10], a reference microphone mounted in proximity of the violin is used to normalize the energy of the sound acquired by the plenacoustic camera with respect to the bowing force acted by the musician. The full 3D pattern is finally obtained by collecting and averaging the contributions coming from all the explored angular regions.

The rest of the paper is structured as follows. In Section 2 we formulate the problem, introducing the notation and the adopted coordinate systems, as well as the theoretical background at the basis of the proposed measurement methodology. In Section 3 we describe the system implementation, providing details about violin tracking, plenacoustic analysis, and the role of the reference microphone. The system validation and the experimental results are discussed in Section 4, while some final considerations are drawn in Section 5.

2. NOTATION AND PROBLEM FORMULATION

2.1. Violin coordinate system

As we are interested in estimating the far field radiation, we consider the violin as a point source located in proximity of the center of mass of the instrument. This position approximately corresponds

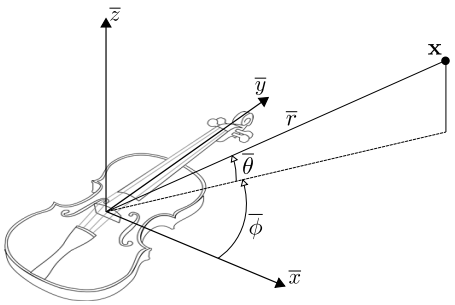

Fig. 1: Violin coordinate system.

to the bridge location, and it is considered as the origin of the violin coordinate system. The coordinate axes are oriented as in Fig. 1, with the bridge lying on the $\overline{x}\overline{z}$ plane. We define the following planes, important for displaying the measured pattern:

- horizontal plane, i.e. the $\overline{x}\,\overline{y}$ plane;
- bridge plane, i.e. the $\overline{x}\,\overline{z}$ plane;
- lateral plane, i.e. the $\overline{y}\,\overline{z}$ plane.

In the paper, we will work also with spherical coordinates, such that a point $\overline{\mathbf{x}}$ is defined by azimuth $\overline{\phi}$, elevation $\overline{\theta}$, and distance $\overline{r}$.

2.2. Radiation pattern

The radiation pattern is defined starting from the far field solution of the Rayleigh's first integral [13]. More specifically, under the far field assumption, the temporal Fourier transform of the radiated sound field at $\overline{\mathbf{x}}$ is given by

$$P(\overline{\mathbf{x}},\omega) = g(\overline{r},\omega)S(\omega)D(\overline{\phi},\overline{\theta},\omega)\,, \qquad (1)$$

where c is the speed of sound, $S(\omega)$ is the temporal Fourier transform of the violin source signal, and ω is the angular frequency; the Green's function

$$g(\overline{r},\omega) = \frac{e^{j\frac{\omega}{c}\overline{r}}}{\overline{r}} \qquad (2)$$

accounts for the propagation delay and attenuation. The term $D(\overline{\phi},\overline{\theta},\omega)$ is the directivity function. The radiation pattern is obtained as $|D(\overline{\phi},\overline{\theta},\omega)|$, and describes the intensity of the sound field emitted towards the direction $(\overline{\phi},\overline{\theta})$ at frequency ω. Notice that for an omnidirectional point source $|D(\overline{\phi},\overline{\theta},\omega)| = 1/(4\pi)$. For arbitrary sources, $0 \leq |D(\overline{\phi},\overline{\theta},\omega)| \leq 1/(4\pi)$.

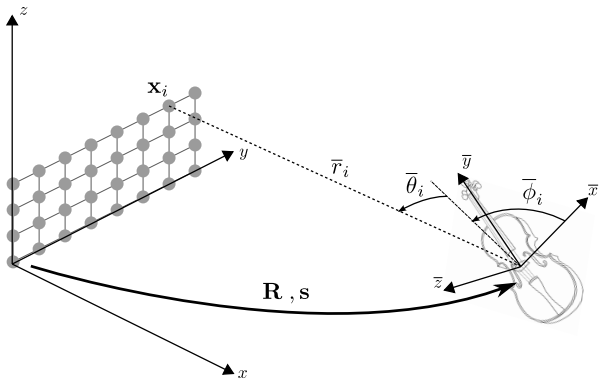

Fig. 2: Plenacoustic analysis.

2.3. Plenacoustic analysis

The goal of this work is to estimate the function $|D(\overline{\phi},\overline{\theta},\omega)|$ for all the frequencies of interest, and covering the full spherical domain defined by the pair $(\overline{\phi},\overline{\theta})$. To do so, we rely on the plenacoustic analysis [12], a powerful tool for determining the directional components of the sound field at multiple points in space. Ideally, a plenacoustic camera is a device that senses the plane wave components contributing to the sound-field at all the points within an aperture [12]. More specifically, this device measures the plenacoustic function $L(\mathbf{x},\mathbf{u},\omega) \in \mathbb{C}$, i.e., the complex amplitude of the ray propagating in the direction of the unit vector $\mathbf{u}$ with respect to the measuring point $\mathbf{x}$. Details of the implementation of this device will be given in Sec. 3.

Since the violin moves and rotates during the measurements, it is useful to define a global coordinate system. Without loss of generality, we choose to locate the global reference frame in correspondence of the camera, as shown in Fig. 2. We sample the plenacoustic function on a regular rectangular grid defined by the points $\mathbf{x}_i$, $i = 1,\dots N$, expressed in the global reference system[1]. Let $\mathbf{s}$ be the position of the violin in the global coordinate system, and $\mathbf{R}$ be the 3×3 matrix defining its rotation with respect to the global reference frame. The point $\mathbf{x}_i = [x_i, y_i, z_i]^T$ can therefore be expressed in the violin coordinate

[1] For the sake of clarity, we mark points in the violin frame using an overline (e.g., $\overline{\mathbf{x}}$), while no symbols are used for points in the global frame (e.g., $\mathbf{x}$).

system as

$$\overline{\mathbf{x}}_i = [\overline{x}_i, \overline{y}_i, \overline{z}_i]^T = \mathbf{R}^{-1}(\mathbf{x}_i - \mathbf{s}) \; . \tag{3}$$

Its spherical coordinates, with respect to the violin reference system, are therefore given by

$$\overline{r}_i = \sqrt{\overline{x}_i^2 + \overline{y}_i^2 + \overline{z}_i^2} = \|\mathbf{x}_i - \mathbf{s}\| \; , \tag{4}$$

$$\overline{\phi}_i = \arcsin\left(\frac{\overline{z}_i}{\sqrt{\overline{x}_i^2 + \overline{y}_i^2 + \overline{z}_i^2}}\right) \; , \tag{5}$$

$$\overline{\theta}_i = \arctan\left(\frac{\overline{y}_i}{\overline{x}_i}\right) \; . \tag{6}$$

This means that the ith sampling point is "illuminated" by the sound radiated by the violin towards the direction $(\overline{\phi}_i, \overline{\theta}_i)$. Assuming that no other acoustic sources radiate from the same direction, we have that

$$L(\mathbf{x}_i, \mathbf{u}_i, \omega) = P(\overline{\mathbf{x}}_i, \omega) = g(\overline{r}_i, \omega) S(\omega) D(\overline{\phi}_i, \overline{\theta}_i, \omega) \; , \tag{7}$$

where $\mathbf{u}_i = (\mathbf{x}_i - \mathbf{s})/\|\mathbf{x}_i - \mathbf{s}\|$ denotes the ray originating at $\mathbf{s}$ and passing through $\mathbf{x}_i$. Inverting this relationship, we compute the radiation pattern at direction $(\overline{\phi}_i, \overline{\theta}_i)$ as

$$\begin{aligned} \left|D(\overline{\phi}_i, \overline{\theta}_i, \omega)\right| &= \left|\frac{L(\mathbf{x}_i, \mathbf{u}_i, \omega)}{g(\overline{r}_i, \omega) S(\omega)}\right| \\ &= \|\mathbf{x}_i - \mathbf{s}\| \frac{|L(\mathbf{x}_i, \mathbf{u}_i, \omega)|}{|S(\omega)|} \; . \end{aligned} \tag{8}$$

3. SYSTEM IMPLEMENTATION

In this Section we describe the system used for estimating the radiation pattern using the relationship in (8). At first, we discuss how the reference microphone is used to select frames containing a violin sound and to estimate the energy $|S(\omega)|$. Then, we describe the tracking system used to estimate the position of the violin $\mathbf{s}$ and its orientation, needed for determining the pair $(\overline{\phi}_i, \overline{\theta}_i)$. Finally, we discuss the implementation of the plenacoustic camera to estimate the term $L(\mathbf{x}_i, \mathbf{u}_i, \omega)$.

Notice that all the measurement devices are mutually synchronized, in order to obtain consistent data.

3.1. Reference microphone

A reference signal $s(t)$ is captured by a microphone located close to the bridge of the violin. As the violin moves and the sound changes its properties during the musical performance, we operate a short-time analysis on $s(t)$. The length of the observation window K is such that, for its duration, the violin can be considered as static and the signal as stationary. We refer to the extracted frame as $s_v(n)$, where n is the discrete-time index and v is the frame index.

In order to discard frames not associated to a violin sound (i.e., related to pauses, or noisy events), or with a poor signal-to-noise-ratio, we perform a frame selection. As we are interested in clean violin sounds, we select only frames characterized by a highly harmonic spectrum, and exhibiting sufficient energy. For each frame we compute the short-time energy

$$e_v = \sqrt{\frac{1}{K} \sum_{n=0}^{K-1} s_v(n)^2} \tag{9}$$

and the harmonic ratio HR_v, calculated using eq.(2.33) in [14]. The harmonic ratio is a non-negative measure of the harmonicity of the spectrum, and the value $\mathrm{HR}_v = 1$ is reached for purely harmonic frames. The vth frame is selected if and only if $e_v \geq T_e$ and $\mathrm{HR}_v \geq T_{\mathrm{HR}}$, where T_e and T_{HR} are prescribed acceptance thresholds.

To obtain an estimate of the amplitude of the source signal at each frequency, we consider the short-time discrete Fourier transform $S_v(\omega_k)$, where ω_k denotes the kth frequency bin.

3.2. Tracking system

In this paragraph we describe the two components of the tracking system, namely an Inertial Measurement Unit (IMU) and a depth map camera. Both the devices are suitably synchronized with respect to the audio recording device. Therefore, all the measurements can be related to the current audio frame v.

IMU A 9-degrees-of-freedom IMU device is used to determine the orientation of the instrument. The device is attached to the chin-rest and positioned such that its local reference frame is oriented as in Fig. 1. The Euler angles (yaw α_v, pitch β_v, and roll γ_v) are obtained by suitably fusing the data measured by 3-axial gyroscope, accelerometer and magnetometer sensors present on the IMU. In particular, we implemented the algorithm in [15] to prevent any

measurement drift. Finally, the violin rotation matrix is obtained from the measured Euler angles as

$$\mathbf{R}_v = \mathbf{R}_z(\alpha_v)\mathbf{R}_y(\beta_v)\mathbf{R}_x(\gamma_v) \ , \tag{10}$$

where $\mathbf{R}_x(\cdot)$, $\mathbf{R}_y(\cdot)$ and $\mathbf{R}_z(\cdot)$ denote the 3D rotation matrices about the x, y and z axes, respectively. As before, the subscript v denotes the frame index.

Depth map camera In order to track the violin position with respect to the global coordinate system, we employ a Microsoft Kinect. The Kinect produces a depth map that it is used to fit a skeleton model, which identifies the pose of the violinist.

We consider the typical pose of a violinist holding the instrument between the left shoulder and the chin. Given the estimated skeleton model, we assume the violin bridge to be located on a line segment originating in correspondence of the chin-rest and directed as the $\overline{y}$-axis of the violin frame. We first estimate the chin-rest position $\mathbf{b}_v$ as the midpoint between the head and the neck skeleton joints. Considering that a standard full size violin has a length of approximately $l = 34\,\text{cm}$, with the bridge located about half the long side of the body, it is therefore reasonable to estimate the bridge position as

$$\mathbf{s}_v = \mathbf{b}_v + \frac{l}{2}\mathbf{y}_v \ . \tag{11}$$

The unit vector $\mathbf{y}_v$ corresponds to the 2nd column of the rotation matrix $\mathbf{R}_v$ computed using (10).

An example of Kinect depth-map and the extracted skeleton joints are shown in Fig. 3. The box in the right picture denotes the violin, drawn according to the position and the orientation estimated by the tracking system.

3.3. Plenacoustic camera

We approximate the ideal plenacoustic camera using $N_r \times N_c = N_m$ omnidirectional microphones arranged as in Fig. 4, and all synchronized with the reference one located on the violin. If we group the microphones in subarrays of $M = 3 \times 3$ sensors, we obtain a grid of $N = (N_r - 2) \times (N_c - 2)$ points on which we can sample the plenacoustic function. To do so, we proceed as follows. Let $\mathbf{x}_i$ be the center of the ith subarray, and $\mathbf{m}_{ij}$, $j = 1, \dots M$, the positions of the sensors within the subarray. The plenacoustic function is estimated through delay-and-sum beamforming [16], i.e., by steering a beam in the direction of the violin and evaluating the corresponding

Fig. 3: Tracking the violin position and orientation.

radiated energy. More specifically, we estimate the energy radiated from the direction

$$\mathbf{u}_i = \frac{\mathbf{x}_i - \mathbf{s}_v}{\|\mathbf{x}_i - \mathbf{s}_v\|} \tag{12}$$

by computing the pseudo-spectrum

$$\psi_v(\mathbf{x}_i, \mathbf{u}_i, \omega) = \frac{\mathbf{a}_v^H(\mathbf{x}_i, \mathbf{u}_i, \omega)\mathbf{\Sigma}_{i,v}(\omega)\mathbf{a}_v(\mathbf{x}_i, \mathbf{u}_i, \omega)}{M^2} \ . \tag{13}$$

In this equation, $\mathbf{\Sigma}_{i,v}(\omega)$ is the covariance matrix of the subarray microphone signals, for the vth frame, and

$$\mathbf{a}_v(\mathbf{x}_i, \mathbf{u}_i, \omega) = \begin{bmatrix} e^{j\frac{\omega}{c}\mathbf{u}_i{}^T(\mathbf{m}_{i1} - \mathbf{x}_i)} \\ \vdots \\ e^{j\frac{\omega}{c}\mathbf{u}_i{}^T(\mathbf{m}_{iM} - \mathbf{x}_i)} \end{bmatrix} \ . \tag{14}$$

The magnitude of the plenacoustic function is finally approximated as

$$|L_v(\mathbf{x}_i, \mathbf{u}_i, \omega)| = \sqrt{\psi_v(\mathbf{x}_i, \mathbf{u}_i, \omega)}. \tag{15}$$

The effect of beamforming is that of minimizing the energy radiated from all directions but that of the desired sound source, i.e., the violin. Therefore, the effect of undesired acoustic reflections turns to be mitigated. This fact makes the plenacoustic analysis suitable for measuring the radiation pattern even in moderately reverberating environments.

3.4. Radiation pattern estimation

Once we have collected all the measurements at frame v, we obtain a set of samples of the function $|D(\overline{\phi}, \overline{\theta}, \omega)|$, which contribute to the estimate of the

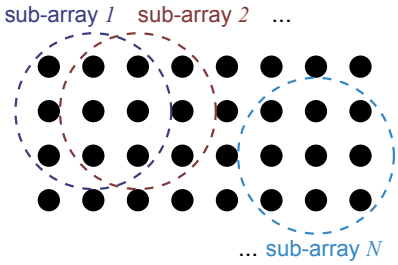

Fig. 4: Plenacoustic camera: implementation.

radiation pattern. More specifically, at frame v we obtain the following samples:

$$\left|D_v(\overline{\phi}_i, \overline{\theta}_i, \omega_k)\right| = \|\mathbf{x}_i - \mathbf{s}_v\| \frac{|L_v(\mathbf{x}_i, \mathbf{u}_i, \omega_k)|}{|S_v(\omega_k)|} , \quad (16)$$

for $i = 1, \dots N$. In order to be robust against measurement noise, we consider only the frequency bins ω_k corresponding to the highest harmonic peaks in the spectrum, i.e., whose energy is not below 20 dB that of the main peak.

At the end of the measuring session, we assume that the violinist moved and rotated in such a way that the radiance pattern has been estimated on the whole 3D angular domain. The gathered data is finally averaged and interpolated to obtain the full 3D pattern, sampled on a regular grid of $N_\phi \times N_\theta = 72 \times 36$ angular positions, i.e., with a resolution of 5° on both the angular axes.

4. RESULTS

In order to verify the effectiveness of the method, we measured the radiation pattern of two different types of acoustic sources. At first, we validated the plenacoustic approach by measuring the pattern of a commercial loudspeaker, whose reference radiation pattern is provided by the manufacturer. Then, we estimated the radiation pattern of a standard full-size student violin. The details of the experiments are reported in the following.

4.1. Acquisition setup

Experiments were conducted in a low-reverberation chamber, with reverberation time $T_{60} \approx 50$ ms. We adopted the T-Bone Ovid CC 100 super-cardiod condenser microphone to measure the reference signal, as described in Sec. 3.1. This sensor is specific for violins and exhibits a sufficiently flat impulse response in the range of interest. The plenacoustic camera has been realized using 32 Beyerdynamics MM1 measurement microphones, characterized by a flat frequency response and by a omnidirectional polar pattern. The microphones are hosted in a pierced wooden plate, covered with acoustic foam. They are arranged on a 4×8 grid as in Fig. 5, so that to obtain $N = 2 \times 6 = 12$ sub-arrays for sampling the plenacoustic function. The microphone spacing is 7 cm in both the horizontal and vertical directions, corresponding to a spatial aliasing frequency of about 2.5 kHz. The camera was disposed with the microphone plane and the microphone rows orthogonal and parallel to the floor, respectively. The Kinect was placed in a calibrated position below the camera, as shown in Fig. 5. The recording sampling frequency was set to 48 kHz. Audio frames were extracted using a $K = 8192$ samples long Hanning window, with 50% overlap. The acceptance thresholds defined in Sec. 3.1 were set to $T_{\mathrm{HR}} = 0.8$ and $T_e = 0.25$.

Fig. 5: Plenacoustic camera and Kinect.

4.2. Radiation of a commercial loudspeaker

As a first test, we measured the horizontal radiation pattern of a Genelec 1029A loudspeaker. The loudspeaker was mounted onto a Outline ET250-3D electronic turntable, and positioned in a calibrated position in front of the camera at a distance of 1.5 m

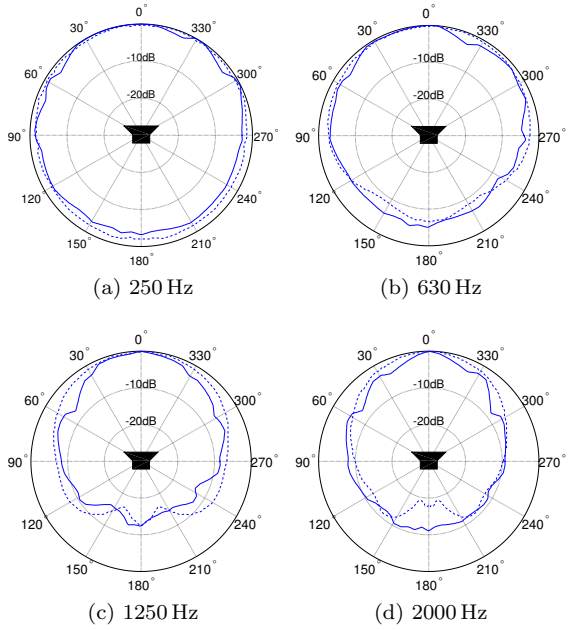

(a) 250 Hz (b) 630 Hz

(c) 1250 Hz (d) 2000 Hz

Fig. 6: Genelec 1029A: measured pattern (continuous line) vs reference pattern (dashed line).

from it. The acoustic center of the loudspeaker (i.e., the midpoint between the woofer and the tweeter) was at the same height of the camera center. In its initial position the loudspeaker was perfectly directed with the cones parallel to the camera, and then rotated clockwise with steps of 10°. In this setup, for each orientation, the loudspeaker is exposed to the camera in an angular range of about 14° in the azimuth and 2° in elevation.

For all the resulting 36 orientations on the full circle, the loudspeaker emitted 2 s of white noise. For this test we omitted the frame selection stage, as the loudspeaker emitted a controlled signal. We also bypassed the tracking system, since the loudspeaker position and orientation were known in advance. To estimate the radiation of the loudspeaker in the horizontal plane, we averaged the results obtained in the two parallel lines of subarrays, corresponding to elevation angles of about ±2°. Comparing the measured pattern with the ground-truth provided by the manufacturer, the resulting average error is below 3 dB in the frequency range 100 Hz - 2.5 kHz. Some examples are reported in Fig. 6, which shows the comparison between the obtained pattern and the ground-truth at four frequency values.

4.3. Radiation of the violin

We estimated the radiation pattern of a full-size student violin in two different experimental scenarios. At first, we instructed the musician to play holding the instrument in a predefined set of positions. In this configuration the pose and rotation of the violin were known, and we bypassed the tracking component of the system. Due to the intrinsic limitations in accurately positioning the instrument held by a person, we limited this analysis to the horizontal plane ($\overline{z} = 0$). More specifically, the musician stood about 1 m from the plenacoustic camera, holding the violin with the plate parallel to the floor. We asked him to rotate in 18 angular prescribed positions, keeping the violin bridge as a pivot. In each position, we violinist played the open D string for approximately 2 s. This way, we obtained a reference measure of the radiation pattern in the horizontal plane. In the second scenario, we tested the whole system (both tracking and audio components). We left the musician free to move, taking care of assuming all the necessary set of positions/rotations for covering the 3D angular range. In each position, the violinist maintained, as much as possible, the standard position of the instrument with respect to his head. We asked him to keep each position for about 2 s, while playing the open D string. To avoid too unnatural poses, we restricted the analysis to the top half sphere of the radiation pattern ($\overline{z} \geq 0$), corresponding to the front side of the violin.

The results of the two experiments are reported in Fig. 7, where the first three rows refer to the horizontal, lateral, and bridge planes, respectively. For the sake of completeness, the last row shows the full 3D pattern as a function of azimuth $\overline{\phi}$ and elevation $\overline{\theta}$. We report the radiation diagrams corresponding to the 5 highest harmonic components of the D note, which in this case were 294 Hz (the fundamental frequency), 588 Hz (first harm.), 882 Hz (second harm.), 1176 Hz (third harm.) and 2058 Hz (seventh harm.). The diagrams are normalized, at each frequency, with respect to the maximum energy radiated in all the sensed directions. The dashed line in the first row of Fig. 7 corresponds to the pattern obtained in the controlled scenario described before. The very good matching between the measured pattern and the reference one reveals the effectiveness

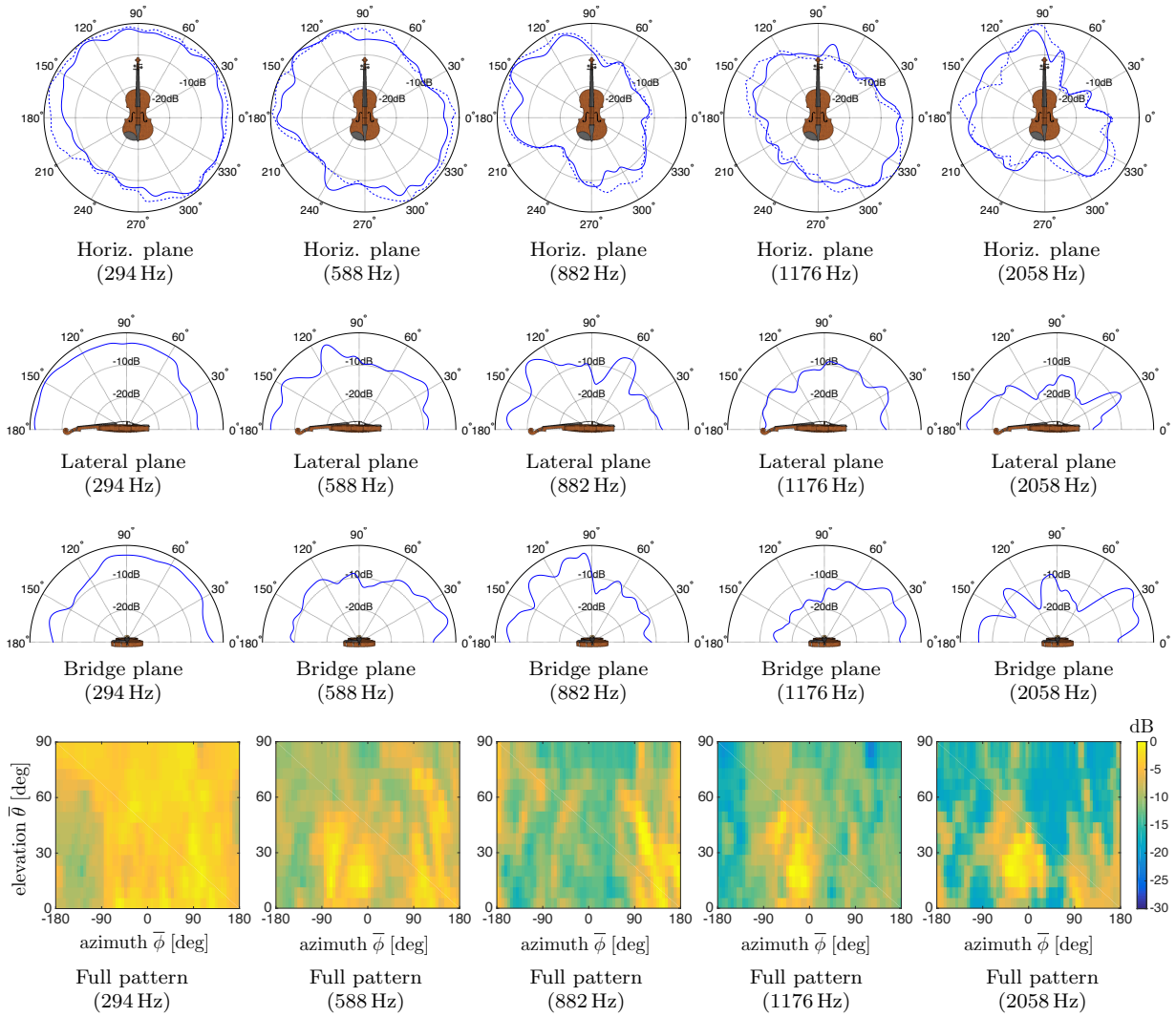

Fig. 7: 3D radiation pattern of the violin under analysis. Results in the horizontal plane are compared with the reference data (dashed line) obtained in a controlled scenario.

of the tracking system.

We first observe that, at 294 Hz and 588 Hz, the radiation pattern is mostly omnidirectional, except for a slight energy damping in correspondence of the violinist's head and neck. Increasing the frequency, the pattern becomes more directive and exhibits more irregular shapes. This behavior agrees with the predictions and results provided by Weinreich in [3], where he found that the transition from a isotropic to a anisotropic radiation occurs approximately at 800 Hz. Indeed, above this frequency the pattern becomes quite unpredictable, confirming that at high frequencies it rapidly changes both in space and frequency. At 1176 Hz there is a clear preferred direction of emission, while at 2058 Hz the pattern presents three main radiation lobes.

It is interesting to note that there is a significant degree of similarity with the radiation diagrams shown in Figs. 4.17-19 of [17]. For instance, the energy damping at 588 Hz in the range $30° - 60°$, in the horizontal plane, is similar to that in Fig. 4.18 of [17] at 550, Hz. Moreover, at 1176 Hz, the main direction

of emission is around 300° in the horizontal plane, which corresponds to that reported in [17]. Similarly, the results present the same trends of those reported in [9]. Naturally, in both the cases, a direct comparison is not possible, as the results in [17] and [9] are relative to different violins. Therefore, we do not expect a perfect match, especially at frequencies above 800 Hz.

Finally, it is worth noticing that the effect of the musician is visible at all frequencies. However, its impact on the radiation becomes relevant at 882 Hz. This frequency corresponds to a wavelength of 39 cm, which starts to be comparable with the head size. It turns that the radiated energy is dimmed down of more than 10 dB in the angular region corresponding to the head ($210° - 240°$ in the horizontal plane, and $\approx 150°$ in the bridge plane).

5. CONCLUSIONS

We have presented a novel methodology to measure the radiation pattern of a violin during the performance, by means of plenacoustic analysis of the radiated soundfield. The radiation pattern is estimated incrementally as the violinist moves and rotates. The directional energy of the soundfield is measured by means of a plenacoustic camera, while the violin position and rotation is tracked through a Kinect and a IMU device.

The proposed method presents several advantages with respect to the state-of-the-art solutions. First of all, the acoustical excitation of the violin is accomplished by a violinist, in order to mimic a concert scenario and to consider the actual effect of the human body on the radiation. Secondly, the tracking system prevents the use of a mechanical positioning device, which would impact on the naturalness of the performance. Thirdly, the plenacoustic method enables measurements even in non-anechoic environments, which are more comfortable for the musicians. Finally, the compact size of the setup minimizes the risk of acoustic interferences (e.g., reflections, diffractions, occlusions) generated by the adopted hardware. The experiments conducted on a known reference loudspeaker confirmed the validity of the measurement method, and the radiated pattern measured from a student violin are perfectly in line with those provided in the literature.

We are currently working on an extension of the system using a second plenacoustic camera located over the violinist, and parallel to the floor. This solution has the advantage of simplifying the acquisition of the back-side radiation pattern, avoiding uncomfortable positions for the musician.

ACKNOWLEDGMENTS

This research activity has been partially funded by the Fondazione CARIPLO (Cultural District of the Province of Cremona), and by the Arvedi-Buschini Foundation. The authors are grateful to the Violin Museum Foundation, Cremona, for supporting the activities of timbral acquisitions on historic violins.

6. REFERENCES

[1] G. Bissinger. Some mechanical and acoustical consequences of the violin soundpost. *The Journal of the Acoustical Society of America*, 1995.

[2] G. Weinreich. Sound hole sum rule and the dipole moment of the violin. *The Journal of the Acoustical Society of America*, 1985.

[3] G. Weinrich. Directional tone color. *The Journal of the Acoustical Society of America*, 1997.

[4] G. Bissinger. Structural acoustics model of the violin radiativity profile. *The Journal of the Acoustical Society of America*, 2008.

[5] G Weinrich and E. Arnold. Method for measuring acoustic radiation fields. *The Journal of the Acoustical Society of America*, 1980.

[6] G. Bissinger and J. Keiffer. Radiation damping, efficiency, and directivity for violin normal modes below 4 khz. *The Journal of the Acoustical Society of America*, 2002.

[7] L. M. Wang and C. B. Burroughs. Acoustic radiation from bowed violins. *The Journal of the Acoustical Society of America*, 2001.

[8] E. Ravina, P. Silvestri, P. Montanari, and G. De Vecchi. Spherical mapping of violins. *The Journal of the Acoustical Society of America*, 2008.

[9] J. Pätynen and T. Lokki. Directivities of symphony orchestra instruments. *Acta Acustica united with Acustica*, 2010.

[10] D. F. Comesana, T. Takeuchi, S. M. Cervera, and K. R. Holland. Measuring musical instruments directivity patterns with scanning techniques. In *International Congress on Sound and Vibration, ICSV*, 2012.

[11] A. Perez Carrillo, J. Bonada, J. Patynen, and V. Valimaki. Method for measuring violin sound radiation based on bowed glissandi and its application to sound synthesis. *The Journal of the Acoustical Society of America*, 2011.

[12] D. Markovic, F. Antonacci, A. Sarti, and S. Tubaro. Soundfield imaging in the ray space. *IEEE Transactions on Audio, Speech, and Language Processing*, 2013.

[13] E. G. Williams. *Fourier Acoustics - Sound radiation and nearfield acoustical holography*. Academic Press, 1999.

[14] H. G. Kim, N. Moreau, and T. Sikora. *MPEG-7 audio and beyond: audio content indexing and retrieval*. Wiley, 2005.

[15] S. O. H. Madgwick, A. J. L. Harrison, and R. Vaidyanathan. Estimation of imu and marg orientation using a gradient descent algorithm. In *IEEE International Conference on Rehabilitation Robotics, ICORR*, 2011.

[16] P. Stoica and R. L. Moses. *Introduction to Spectral Analysis*. Prentice Hall, 1997.

[17] J. Meyer. *Acoustics and the performance of music: manual for acousticians, audio engineers, musicians, architects and musical instruments makers*. Springer, PPV Medien, 2009.